The effect of thermal oxidation on laser-induced photoelectron emission during tensile deformation of polycrystalline aluminum

M. Cai,[1,2,a] R. E. Ricker,[3] L. E. Levine,[3] S. C. Langford,[1] and J. T. Dickinson[1]
[1]*Department of Physics and Astronomy, Washington State University, Pullman, Washington 99164, USA*
[2]*School of Materials Science and Engineering, Southeast University, Nanjing 211189, China*
[3]*National Institute of Standards and Technology, 100 Bureau Drive, Gaithersburg, Maryland 20899, USA*

(Received 28 September 2009; accepted 23 January 2010; published online 12 March 2010)

Many metals emit electrons when exposed to UV radiation (photon energies 4 to 8 eV). Deformation can significantly affect the intensity of these emissions. In the case of reactive metals, these emissions are also altered by the presence of surface oxides. We have characterized the effect of thermal oxides on laser-induced photoelectron emission from commercially pure polycrystalline aluminum with a view toward using these emissions as a probe of deformation processes. The thickness of oxides produced by a range of annealing treatments in air was determined by x-ray photoelectron spectroscopy. Time-of-flight measurements on photoelectrons from these surfaces under 248 nm irradiation (5 eV photons) show two peaks: a fast peak which we attributed to electrons from metallic aluminum, and a slower peak, which may be due to electrons from interface states. Surface oxide films of sufficient thickness attenuate both peaks. We show that the sensitivity of the photoelectron signals to deformation varies with thermal oxidation pretreatments and oxide film thickness and that with the appropriate oxide thickness the total photoelectron intensity becomes a sensitive probe of deformation-related processes during tensile testing. © *2010 American Institute of Physics*. [doi:10.1063/1.3327237]

I. INTRODUCTION

Electron emission from metal surfaces depends strongly on the details of atomic bonding at the surface and this may be exploited to probe changes in the surface due to mechanical deformation. Electron emission induced by reactions between metallic alloys and electronegative gases[1–6] has been exploited to probe the production of fresh metal surface during the tensile deformation of titanium and zirconium in oxygen.[7] Electron emission due to photoelectronic processes is also affected by deformation.[8,9] Photoemission due to the intersection of slip steps with the surface[10–13] and cracks in nonmetallic surface coatings[14,15] is readily observed. In some systems, the intensity and nature of photoelectron signals from aluminum alloys can be exploited to assess the nature of the oxide film.[16]

Photoemission images during fatigue testing have provided significant insights into the progress of deformation,[15,17] although the complexity of deformation in fatigue complicates quantitative analysis. Time-resolved photoemission measurements during simpler tensile deformation experiments have been generally restricted to small strains and have provided little real-time information on the progress of deformation. In this work, we describe attempts to optimize the information derived from laser-induced photoelectron emission measurements during deformation by investigating the influence of thermal oxidization pretreatments.

We examine the effect of thermal oxidation on photoelectron emission from annealed, commercially pure aluminum during irradiation with a pulsed excimer laser (KrF, $\lambda = 248$ nm). Oxidation was performed in air for periods of 0.5 to 10.0 h at temperatures of 200, 300, 400, and 500 °C. X-ray photoelectron spectroscopy (XPS) was employed to characterize the resulting oxides. Time-of-flight (TOF) measurements on the laser-induced photoelectron emissions show two distinct peaks: a faster peak that grows during deformation and a slower peak that does not. The goal is to identify the oxidation treatment that optimizes the sensitivity of the photoelectron signals to deformation-induced changes in the surface of pure Al.

II. EXPERIMENT

Dog-bone shaped tensile specimens were cut from 1 mm thick, annealed, commercially pure Al (>99.95% mass fraction) sheet. The gauge section was of 25.4×5 mm^2, with the long dimension parallel to the rolling direction of the sheet. Samples were polished, ultrasonically cleaned, and thermally oxidized in air at 200, 300, 400, or 500 °C, respectively for periods ranging from 0.5 to 10.0 h. Tensile deformation was carried out in vacuum ($<10^{-7}$ Pa) at a constant crosshead speed of 0.125 mm/s. The failure strains for these samples tested in this manner ranged from 33.6% to 38.6%.

XPS was employed to determine the thickness of the thermal oxides. Spectra were acquired with a Kratos Axis 165 (Ref. 18) photoelectron spectrometer using a dual Mg K_α source. The hemispherical electron energy analyzer was operated in the electrostatic magnification, fixed analyzer, and transmission mode. Electron intensities were measured at kinetic energy increment of 0.1 eV with a pass energy of 40 eV.

[a]Author to whom correspondence should be addressed. Present address: Exova Group Ltd., 9925 Regal Row, Houston, TX 77040. Electronic addresses: mingdong.cai@exova.com and mingdongcai@hotmail.com.

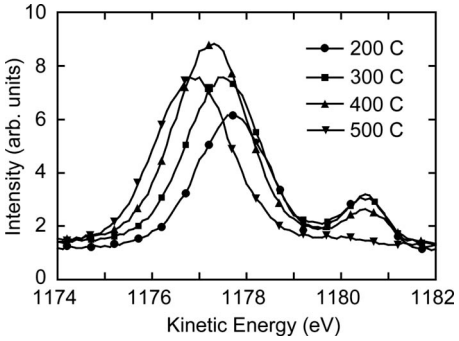

FIG. 1. XPS spectra of aluminum annealed in air at 200, 300, 400, and 500 °C for 3 h with half of the data points shown and fitting curves added. The peak on the left is due to Al $2p$ photoelectrons from aluminum oxide and the peak on the right is due to Al $2p$ photoelectrons from aluminum metal. The estimated uncertainty in these measurements is less than the size of the data points (0.084 arbitrary units).

Photoelectron measurements were performed in a stainless steel vacuum system at a pressure of 1×10^{-7} Pa by illuminating an area about 3×9 mm^2 on one side of the tensile specimen that included the region where strain localization and necking occurred. Electron emission was monitored with a Burle Electro-Optics Model 4716 Channeltron electron multiplier mounted 150 mm from the sample (near normal to the sample gauge plane) and operated at a gain of about 10^6.

Pulses with a wavelength of 248 nm and duration of 30 ns were provided by a Lambda Physik Lextra 200 excimer laser operated at a repetition rate of 2 Hz. The laser beam was attenuated with a Micro Las variable attenuator and two 5% transmission filters to achieve a total fluence of 500 μJ/cm^2 at the sample gauge section. Atomic force microscopy showed no evidence of laser-induced damage at this low fluence. The fluence threshold for surface damage by 248 nm light on these samples (corresponding to the formation of a plasma) is about 1 J/cm^2.

After tensile deformation, portions of the deformed gauge sections were imaged with a JEOL-6400 scanning electron microscope (SEM) operated at an accelerating voltage of 20 kV. Atomic force microscopy (AFM) images of the deformed surfaces were acquired with a Digital Instruments (Santa Barbara, CA) Nanoscope III multimode scanning probe microscope operated in the contact mode. The SEM and AFM images are from the uniformly deformed region of the gauge section 2.5 mm or more away from the tensile fracture.

III. RESULTS AND DISCUSSION

A. Oxide characterization by XPS

Figure 1 shows typical XPS spectra of undeformed aluminum annealed in air for 3 h at four different temperatures. This range of binding energies includes photoelectrons from Al $2p$ states. The smaller peak at the lower binding energy on the right corresponds to photoelectrons from metallic aluminum, while the larger peak at the higher binding energy on the left corresponds to photoelectrons from aluminum ions in the oxide. At constant annealing time, increasing the annealing temperature increases the oxide thickness, thereby increasing the intensity of photoelectrons from the oxide. Because electrons from the underlying metal are attenuated in the oxide by inelastic scattering events, increasing the oxide thickness decreases the intensity of the photoelectrons from the metal. The metallic peak after a 500 °C anneal is hardly visible due to the thick oxide.

The position of the metallic peak remains unchanged as the overlying oxide grows thicker. Similarly, the low binding energy edge of the oxidic peaks for the samples annealed at 200 to 400 °C virtually overlap. However, the high binding energy side of the oxidic peaks shifts to higher binding energies (to the left) with increasing oxide thickness. The details of this shift are beyond the scope of this work but reflect variations in the electrostatic potential through the thickness of the oxide film.[19,20] The low binding energy photoelectrons arise from states close to the metal-oxide interface, where the electron potential energy is relatively high. As one moves away from the interface, the electron potential energy decreases and the binding energy increases.[21,22] As the oxide thickness increases, the fraction of Al $2p$ photoelectrons originating from high binding energy sites increases—and the oxidic peak shifts to higher binding energies.

Although x-ray photoelectrons from Al $2p$ states are emitted with well-defined energies relative to the local electrostatic potential, these electrons can excite bandgap or plasmon excitations and lose energy as they pass through the oxide film. Electrons that have generated these excitations can generate separate peaks but more generally they contribute to the background. The intensity of electrons that pass through the oxide film without generating excitations decreases exponentially with increasing oxide thickness. With very thick oxides, few photoelectrons from the metal substrate reach the detector. This is the case for the sample annealed at 500 °C, where the metallic Al $2p$ peak is quite small.

For oxide thicknesses on the order of the electron attenuation length, the thickness of the oxide layer can be estimated by comparing the Al $2p$ photoelectron intensities (peak areas) from the oxide (I_O) and the metal (I_M).[23–28] The Al $2p$ photoelectrons generated by Mg K_α radiation have mean free paths of $\lambda_O=2.42$ nm ±0.15 nm in the oxide and $\lambda_M=2.23$ nm ±0.13 nm in the metal, respectively.[25,27] Photoelectron production is roughly proportional to the number of aluminum atoms per unit volume: $N_O=0.07$ to 0.09 mol/cm^3 (depending on the oxide) and $N_M=0.100$ mol/cm^3. Assuming an oxide density on the low end ($N_O=0.07$ mol/cm^3) and that the photoelectrons pass through the oxide normal to the surface ($\theta=90°$), the oxide thickness estimate d is[25]

$$d=\lambda_O \sin\theta \ln\left[\left(\frac{N_M\lambda_M}{N_O\lambda_O}\right)\left(\frac{I_O}{I_M}\right)+1\right]$$
$$\approx 2.4\ln\left[1.3\left(\frac{I_O}{I_M}\right)+1\right]. \quad (1)$$

Strohmeier estimates that the uncertainty in the resulting oxide film thickness is about 0.10 nm.[25]

The photoelectron intensities I_O and I_M were determined by curve fitting the background and photoelectron peaks and

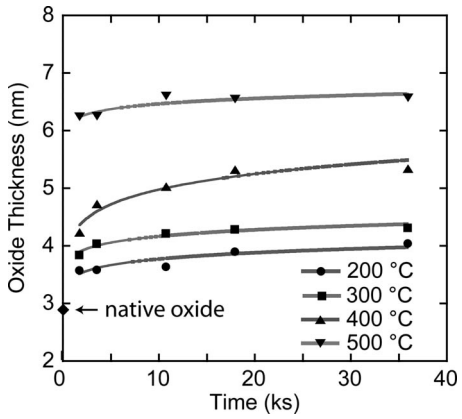

FIG. 2. Estimated oxide thicknesses as a function of anneal duration at temperatures of 200, 300, 400, and 500 °C. The curves are empirical fits to an equation of the form t^M, where t is the annealing time; the estimated uncertainty (see text) is less than the size of the data points.

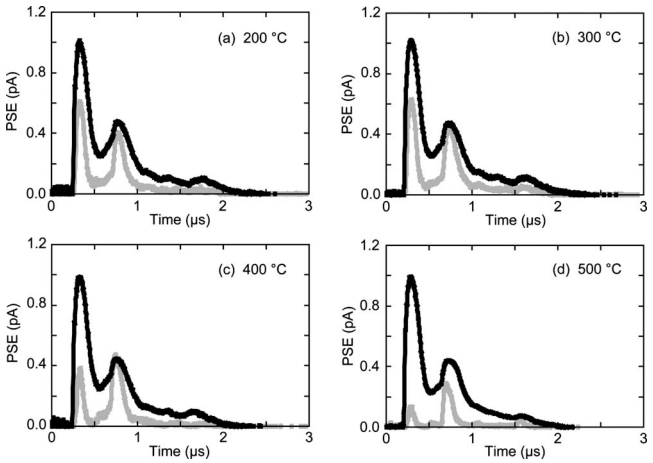

FIG. 3. Laser-induced photoelectron emission signals vs time due to single laser pulses before (gray line) and after (black line) tensile deformation to failure of aluminum oxidized at (a) 200 °C, (b) 300 °C, (c) 400 °C, and (d) 500 °C for 3 h.

estimating the area under the peaks from the curve fit parameters. We note that this treatment, although standard, neglects any sample-to-sample variability in oxide composition, as well as the excitation of intrinsic surface and bulk plasmons in the metal substrate.[28] Thus, the oxide thickness estimates reported below are likely to be somewhat high.

The oxide thicknesses calculated from Eq. (1) are plotted as a function of oxidization time in Fig. 2 for the four annealing temperature employed in this work. The general features of the growth curves, including the rapid growth to a limiting thickness, are typical of oxide growth in this system.[28] However, quantitative agreement is not expected because our samples are annealed in air (high oxygen partial pressure) and are covered with a significant native oxide (≈2.9 nm, see also Fig. 2) prior to annealing. As expected, the limiting thickness increases as the annealing temperature increases. Interestingly, the oxide grown at 400 °C takes significantly longer to reach its limiting thickness than the oxides grown at the other temperatures. This continuous growth allows for relatively high defect densities along the metal/oxide interface, even after 5 h at 400 °C. As discussed below, this would account for the relatively high intensities of slow photoelectrons from oxides annealed at 400 °C.

B. Photoelectron TOF signals versus annealing temperature

Metals yield photoelectrons when exposed to photons with energies greater than their work function—about 4.3 eV for bare polycrystalline aluminum. Although the commercial, oxidized material employed here is not clean by surface science standards, photoemission is observed when the material is exposed to 248 nm (5.0 eV) photons from a pulsed excimer laser. The duration of each laser pulse is only 30 ns, allowing for meaningful measurements of the time required for the electron to travel to the detector. Typical electron TOF signals accompanying a single, 248 nm laser pulse appear in Fig. 3. The gray curves were acquired before tensile testing and the dark curves were acquired after tensile testing (sample pulled to failure). Each TOF signal shows two peaks: the faster peak arrives about 0.3 μs after the laser pulse and the slower peak about 0.7 μs after the laser pulse. After failure, the intensity of the fast peaks from each sample is increased but the position (time) of the peak is unchanged.

The kinetic energy of the electrons comprising these two peaks was estimated by modeling the electron trajectories. The electrostatic potentials in the region between the grounded sample and the electron detector were determined by solving Laplace's equation with boundary conditions appropriate for our experimental geometry.[29–32] Trajectories and transient times for single electrons with a variety of initial kinetic energies and launch angles were calculated and compared with the observed transient times. These simulations show that the detected electrons are emitted in a narrow cone confined to angles within 10º of the surface normal and travel along nearly straight-line paths to the detector. The best agreement between experimental and simulated transient times was obtained for initial electron kinetic energies of approximately 0.7 and 0.05 eV for the fast and slow peaks, respectively. The kinetic energy of the fast peak is consistent with the difference between the photon energy (5 eV) and the work function of aluminum, typically 4.1 to 4.4 eV depending on crystallographic orientation. This suggests that the fast electrons are emitted from the metallic phase through surface oxide structure without losing energy.

The origin of the slow peak is not clear. If this peak was due to emission originating from defect states within the oxide, the magnitude of this peak should increase with oxide thickness, which is not observed. The observed behavior is consistent with a low density of suitable states for emission in the interior of the film and a relatively high density of defects along the metal-oxide interface, as expected.[33] Charge transfer from the metal to oxide interface states typically yields filled interface states just below the metal Fermi level.[34,35] Such states would be suitable initial states for photoemission.

C. Photoelectron intensity versus oxide thickness

Although aluminum oxide is effectively transparent to 248 nm photons, a sufficiently thick oxide can hinder the

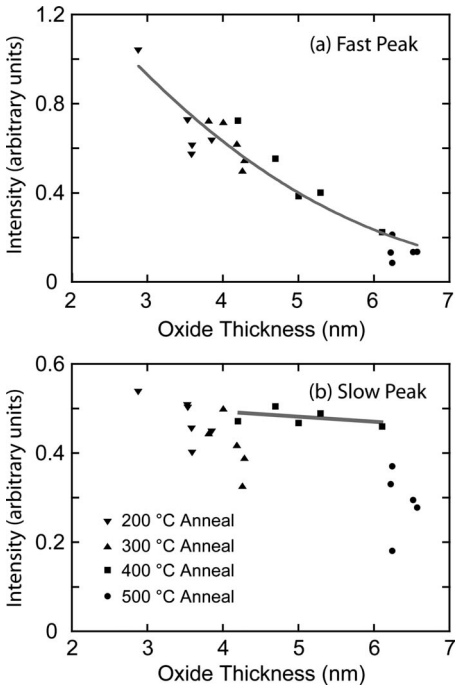

FIG. 4. (a) Fast peak and (b) slow peak photoelectron intensities as a function of oxide thickness (as determined by XPS). The curve in (a) represents a least-squares fit of all the data to an exponential decay with a decay constant of 3.3 nm. The gray line in (b) guides the eye through the data points corresponding to the oxide formed at 400 °C. The measurement uncertainties are the same as in Figs. 1 and 2.

escape of electrons from the underlying metal. The intensities of the fast and slow peaks are shown in Fig. 4 as a function of oxide thickness as determined by XPS and Eq. (1). The overall drop in the fast peak intensity with oxide thickness is well described by an exponential decay with an attenuation length of about 3.3 nm. This is comparable to the attenuation length of 1.0 for 150 nm photons determined by Buzulutskov *et al.*[36] for alumina films vacuum deposited on CsI, where somewhat higher electron kinetic energies are expected. It is also (coincidentally) comparable to the attenuation length of the XPS photoelectrons described above (λ_O=2.4 nm). A longer attenuation length of 14 nm was reported by Pong on anodized aluminum illuminated by 122 nm photons,[33] possibly due to the porosity of the thicker, anodized films. Although the slow peak intensity varies considerably with anneal time (independent of oxide thickness), a similar analysis of attenuation yields an attenuation length of about 7 nm.

In contrast with XPS photoelectrons, the kinetic energies of UV photoelectrons are far too low (<1 eV) to generate bandgap or plasmon excitations in the oxide (≥9 eV). The most important potential excitation at these photoelectron energies are surface plasmons (Fuchs–Kliewer modes), whose energies (typically near 0.1 eV for aluminum oxide) and excitation probabilities depend on oxide thickness.[37] The long phonon wavelength and the long range of the associated dipole electric field render these interactions relatively *insensitive* to submicron inhomogeneities. The surface plasmons on aluminum oxide are also relatively insensitive to the crystalline form of the oxide. High resolution electron energy loss spectroscopy studies of aluminum surfaces oxidized in partial vacuum show significant energy loss peaks near 0.06 and 0.10 eV as the film thickness increases above 3 nm.[38,39] Thus we expect that electrons in the fast peak would excite surface plasmons. The corresponding scattering process for electrons in the slow peak would be much weaker. This would explain why the slow peak intensity falls more slowly with oxide thickness than the intensity of the fast peak.

The fast and slow electron intensities decrease significantly (up to 40%) with anneal time at anneal temperatures of 200 and 300 °C, despite the small changes in oxide thickness at these temperatures. The common behavior suggests a common attenuation mechanism. It is unlikely that this mechanism is inelastic scattering, due to the contrasting electron kinetic energies of the two peaks. However, both fast and slow electrons would respond significantly to small changes in the apparent work function during annealing. In the aluminum/aluminum oxide system, decreasing the density of interface states (electron traps and oxygen vacancies[40]) increases the apparent work function by reducing the amount of charge transfer required to align the metal and oxide Fermi levels.[40]

At the annealing temperatures employed in this work, defects along the metal-oxide interface are formed and reformed continuously during oxide growth, as aluminum ions migrate from the metal through the existing oxide to the oxide surface. In the absence of growth, annealing generally reduces defect densities, including those along the interface. Annealing improves the crystallinity and stoichiometry (relative to γ-alumina) of oxide films on aluminum over the entire range of annealing temperatures employed in this work.[21,41] Almost all the annealing at 200 and 300 °C (but not 400 °C) occurs after the oxide has stopped growing (see Fig. 2); thus it is reasonable to expect the density of interfacial defects to decrease during the lower temperature anneals but not at 400 °C. This would account for the drop in fast and slow peak intensities with increasing anneal time at 200 and 300 °C, despite the lack of oxide growth. At 400 °C, annealing continuously increases the film thickness and would continuously regenerate interface states; as the oxide grows, the apparent work function would remain relatively low but inelastic scattering would increasingly attenuate the fast electrons. Since the slow electrons lack the kinetic energy to excite most inelastic processes, the slow electron peak would be only weakly attenuated after prolonged annealing at 400 °C. Significant attenuation in both fast and slow peak intensities appear in the samples with oxide thickness greater than 6 nm—e.g., for the oxides formed by annealing at 500 °C in Figs. 2–4.

Assuming that the slow electrons originate from interface states, any reduction in interface state density will directly reduce the slow peak intensities. However, both fast and slow electron intensities depend exponentially on the apparent work function, leading one to expect that these changes are the dominant effect. Kuznetsova found that the work function of oxide films formed during exposure to low pressure ozone was 0.23 eV higher than films formed in oxygen—again attributed to a lower density of oxygen vacancies along the interface.[40] Smaller changes in the appar-

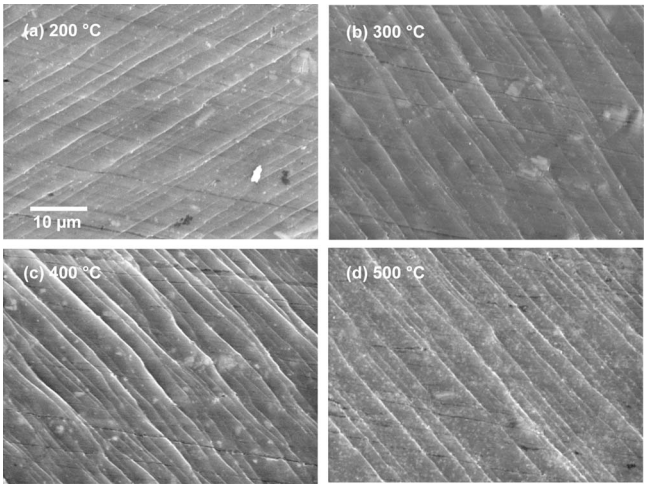

FIG. 5. SEM images of aluminum samples acquired after deformation in tension to failure. The samples were annealed for 3 h in air at temperatures of (a) 200 °C, (b) 300 °C, (c) 400 °C, and (d) 500 °C. In each case, the imaged area is located at least 2.5 mm from the fracture surface.

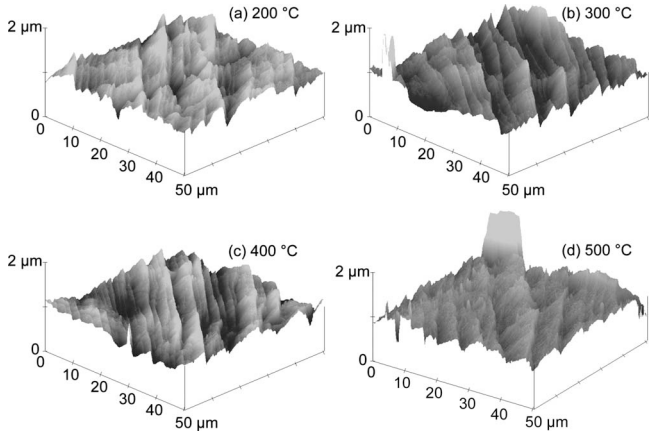

FIG. 6. AFM images of aluminum samples acquired after deformation in tension to failure. The samples were annealed for 3 h in air at temperatures of (a) 200 °C, (b) 300 °C, (c) 400 °C, and (d) 500 °C. In each case, the imaged area is located at least 2.5 mm from the fracture surface.

ent work function would easily account for the decrease in fast and slow peak intensities after annealing at 200 and 300 °C.

D. Photoelectron emission during deformation

During tensile deformation of aluminum, much of the plastic strain is accommodated by cooperative dislocation motion and the formation of slip bands. Typical SEM images of the uniformly deformed gauge section of the aluminum samples after deformation in tension to failure (≈36% strain) are shown in Fig. 5. The distinct diagonal features in each image are where regions of intense dislocation activity, known as slip bands, intersect the surface. For a metallic alloy covered with an oxide film, the formation of slip steps exposes bare metal. Outside of a vacuum, oxide reforms on these freshly exposed slip steps; but in a vacuum, these areas will remain bare and UV illumination should result in photoemission from the surface that increases as the growth of these steps exposes more bare metal.

The geometry of the new surfaces exposed by slip is clearer in AFM images of the annealed surfaces acquired after failure, shown in Fig. 6. Most of the steps in these images are several tens of nanometers high—significantly higher than the oxide film thicknesses in this work. Therefore, most of the fresh metal projects above the oxide layer, and photoelectrons can be emitted directly into vacuum without passing through the oxide. Using anodized aluminum, Arnott and Ramsey[1] detected significant increases in electron emission during the deformation of samples with average oxide thicknesses below 45 nm. We have previously reported changes in laser-induced electron emission intensities accompanying plastic deformation of several Al alloys[32] and single crystals[42] with native oxide coatings.

Figure 7(a) displays a typical smoothed stress and photoelectron signals as a function of applied strain acquired during testing of an aluminum tensile specimen oxidized for 3 h at 400 °C. Each data point in the photoelectron signal represents the total charge delivered by the electron multiplier after a laser pulse; this total charge corresponds to the area under a single electron TOF curve in Fig. 4. The behavior of the photoelectron signal can be divided into four regimes based on the slope of this curve. In the first region (from 0% to ≈4% strain), the photoelectron signal is constant during elastic deformation and continues to be nearly constant well after the first signs of plastic deformation. Then, after about 2% or 3% strain, when plastic deformation has become widespread and uniform, the photoelectron signal starts to increase linearly with plastic strain. This second region of rapid work hardening continues up to 15% to 20% strain where as the slope of the stress-strain curve starts to approach zero. At this point, the slope of the linear photoelectron signal as a function of strain changes, and this marks the beginning of the third region. In the third region, the photoelectron signal continues to increase linearly with strain

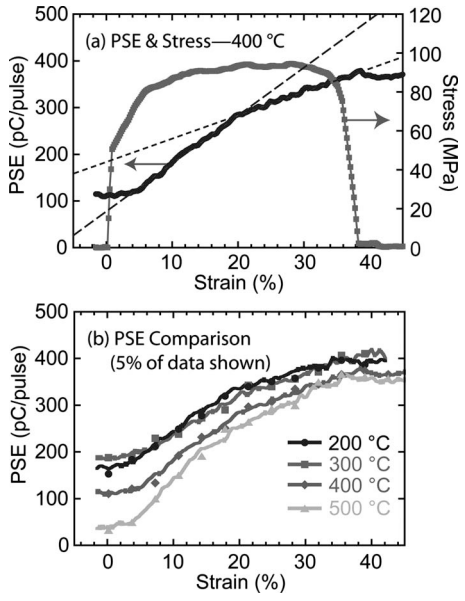

FIG. 7. (a) Smoothed strain and photoelectron signals acquired during tensile testing of an aluminum sample oxidized at 400 °C for 3 h. (b) Photoelectron signals acquired during testing of samples oxidized at 200, 300, 400, and 500 °C for 3 h. The strains at failure ranged from 33.6% to 38.6%.

but at a lower slope than that observed in second region. This behavior continues until separation of the fracture surface is complete. The fourth region is observed after the last ligament of the fracture surface is completely torn; the rate of bare surface generation drops to zero and the photoelectron emission intensity becomes constant.

A small increase in the photoelectron signal during the first region would be expected for several reasons, including oxide cracking due to elastic stresses, dislocation motion prior to the onset of general plastic deformation,[43,44] and a small decrease in the work function as the strain/stress increases.[45] The change in signal intensity in this region is small and continues to be small until well after the onset of plastic deformation (at about 0.05% for the modulus and yield strength of pure Al). This behavior could be due to the irregular nature of the early stages of plastic deformation or the small opening displacements in the oxide film for these low levels of plastic strain.[46]

As deformation proceeds to the second region, working hardening in the grains favorably oriented for slip locally stiffens these grains until the yield strength is exceeded in all of the grains and uniform plastic deformation results. Once deformation becomes uniformly distributed, the imposed strain rate must equal the plastic strain in the tensile axis; if not, the stress increases (nucleating more slip bands) until it does. Under these conditions, the fraction of the illuminated area composed of bare metal should increase linearly with strain, accounting for the linear growth of photoelectron intensity with strain.[32]

Eventually, work hardening results in strain localization and the formation of a thin (necked) region in the gauge section. Once necking initiates, virtually all subsequent plastic strain is confined to the region of the neck. In this third region of deformation, the rate of surface area production is still proportional to the strain rate but much of the new surface appears on the thin (1 mm thick) edges of the gauge section, which are not illuminated by the laser. Thus, the photoelectron signal still increases linearly with strain but the rate of increase (the slope of the curve) decreases. The dotted lines in Fig. 7(a) show the linear regions of photoelectron signal growth before and after the onset of strain localization. The onset of strain localization coincides with the inflection point in the photoelectron signal.[32] In some case it is easier to identify the onset of localization from the inflection point in the photoelectron signal than the strain data.[32] Large changes in the photoelectron signal can occur at fracture if the bare metal of the serrated fractured surface becomes exposed to the laser.

Figure 7(b) shows typical photoelectron signals acquired during tensile testing of samples annealed for 3 h at temperatures of 200, 300, 400, and 500 °C. The strains at failure ranged from 33.6% to 38.6%. Each signal shows the three stages of deformation illustrated in Fig. 7(a). Importantly, the photoelectron intensity prior to deformation *decreases* dramatically as the annealing temperature increases. This is consistent with the strong dependence of photoemission intensity on oxide thickness and annealing temperature in Fig. 2.

Ultimately, our goal is to increase the sensitivity of our photoelectron measurements to the point where the production and growth of individual slip bands can be detected. The optimum surface treatment for these experiments will provide an oxide thick enough to attenuate photoelectron emission from the gauge section prior to deformation but thin enough to allow for efficient detection of electrons emitted from nearby deformation-induced metal surfaces. Under the experimental conditions of this work, an oxide layer about 4 nm thick, produced by a 3 h anneal at 300 °C, provided the best results. Longer anneals at 300 °C yield less uniform oxides, due to the uneven progress of oxidation and crystallization within the film.[21,28,41,47,48] Annealing samples at higher temperatures yielded films that were too thick. Further, it has been found from this work that the intensity of the fast photoelectron signal can be used to estimate the thickness of the oxide layer given appropriate standards.

IV. CONCLUSIONS

Annealing commercially pure polycrystalline aluminum in air produces a thermal oxide that has important effects on photoelectron emission before and during tensile testing. XPS measurements of oxide thickness show the expected growth kinetics as a function of temperature and duration of anneal.[41] Electron TOF measurements show two prominent peaks. The faster of these peaks is consistent with emission from metallic aluminum and decays exponentially with increasing oxide thickness. The slower of these peaks is more weakly attenuated as the oxide thickness increases. After the oxide reaches a limiting thickness (low temperature anneals only), both peaks generally grow weaker with increasing annealing times. We suggest that the slow electrons arise from states at the metal-oxide interface. Photoemission measurements during tensile testing show rising emission intensities due to the bare patches of metal produced by deformation. These signals reflect the progress of incipient and linear deformation, followed by strain localization and failure. The oxide thickness dependence of the photoemission intensities during deformation demonstrates that an oxide thickness of 4 nm provided optimum conditions for strong photoemission while minimizing the background photoelectron signal due to undeformed material. Laser-induced photoelectron emission during deformation promises to provide useful, real-time information concerning surface microstructural changes during deformation.

ACKNOWLEDGMENTS

This work was supported by Department of Energy under Grant No. DE-FG02-02ER45988. We thank Chase Bradford, Washington State University, for programming the electron trajectory simulations.

[1] D. R. Arnott and J. A. Ramsey, Surf. Sci. **28**, 1 (1971).
[2] B. Kasemo, E. Törnqvist, J. K. Nørskov, and B. I. Lundqvist, Surf. Sci. **89**, 554 (1979).
[3] J. K. Nørskov, D. M. Newns, and B. I. Lundqvist, Surf. Sci. **80**, 179 (1979).
[4] R. H. Prince, R. M. Lambert, and J. S. Foord, Surf. Sci. **107**, 605 (1981).
[5] M. P. Cox, J. S. Foord, R. M. Lambert, and R. H. Prince, Surf. Sci. **129**, 399 (1983).
[6] E. B. D. Bourdan and R. H. Prince, Surf. Sci. **144**, 591 (1984).
[7] J. T. Dickinson, L. C. Jensen, and S. C. Langford, J. Mater. Res. **9**, 1156

(1994).
[8]V. S. Kortov and R. I. Mints, FKhMM [Soviet Matter. Sci.] **2**, 272 (1966).
[9]T. K. G. Swami and Y. W. Chung, Surf. Sci. **99**, 373 (1980).
[10]W. J. Baxter and S. R. Rouze, J. Appl. Phys. **44**, 4400 (1973).
[11]W. J. Baxter, J. Appl. Phys. **45**, 4692 (1974).
[12]W. J. Baxter and S. R. Rouze, J. Appl. Phys. **46**, 2429 (1975).
[13]O. Buck, W. J. Pardee, F. J. Szalkowski, and D. O. Thompson, Appl. Phys. (Berlin) **12**, 301 (1977).
[14]W. J. Baxter, Vacuum **22**, 571 (1972).
[15]W. J. Baxter, J. Appl. Phys. **44**, 608 (1973).
[16]J. T. Dickinson, P. F. Bräunlich, L. A. Larson, and A. Marceau, Appl. Surf. Sci. **1**, 515 (1978).
[17]W. J. Baxter and S. R. Rouze, Metall. Trans. A **7A**, 647 (1976).
[18]Commercial equipment and materials are identified in this work in order to adequately specify certain procedures. In no case does such identification imply recommendation or endorsement by the National Institute of Standards and Technology or Washington State University, nor does it imply that the materials or equipment identified are necessarily the best available for the purpose.
[19]J. C. Fisher and I. Giaever, J. Appl. Phys. **32**, 172 (1961).
[20]S. R. Pollack and C. E. Morris, J. Appl. Phys. **35**, 1503 (1964).
[21]L. P. H. Jeurgens, W. G. Sloof, F. D. Tichelaar, and E. J. Mittemeijer, Surf. Sci. **506**, 313 (2002).
[22]P. C. Snijders, L. P. H. Jeurgens, and W. G. Sloof, Surf. Sci. **589**, 98 (2005).
[23]R. Holm, Vackuum Technik **23**, 208 (1974).
[24]R. Holm and S. Storp, J. Electron Spectrosc. Relat. Phenom. **8**, 139 (1976).
[25]B. R. Strohmeier, Surf. Interface Anal. **15**, 51 (1990).
[26]I. Olefjord, H. J. Mathieu, and P. Marcus, Surf. Interface Anal. **15**, 681 (1990).
[27]H. Yamamoto, Y. Baba, and T. A. Sasaki, Surf. Sci. **349**, L133 (1996).
[28]L. P. H. Jeurgens, W. G. Sloof, F. D. Tichelaar, C. G. Borsboom, and E. J. Mittemeijer, Appl. Surf. Sci. **144–145**, 11 (1999).
[29]K. Binns and P. Lawrenson, *Analysis and Computation of Electric and Magnetic Fields Problems*, 2nd ed. (Pergamon, New York, 1973).
[30]R. W. Stanley, Am. J. Phys. **52**, 499 (1984).
[31]M. E. Peskin, Comput. Sci. Eng. **5**, 92 (2003).
[32]M. Cai, S. C. Langford, L. E. Levine, and J. T. Dickinson, J. Appl. Phys. **96**, 7189 (2004).
[33]W. Pong, J. Appl. Phys. **40**, 1733 (1969).
[34]A. M. Ferendici, *Physical Foundations of Solid State and Electron Devices* (McGraw-Hill, New York, 1991).
[35]E. H. Rhoderick and R. H. Williams, *Metal-Semiconductor Contacts* (Claredon, Oxford, 1998).
[36]A. Buzulutskov, A. Breskin, and R. Chechik, J. Appl. Phys. **81**, 466 (1997).
[37]R. Fuchs and K. L. Kliewer, Phys. Rev. **140**, A2076 (1965).
[38]M. Liehr, P. A. Thiry, J. J. Pireaux, and R. Caudano, J. Vac. Sci. Technol. A **2**, 1079 (1984).
[39]B. G. Frederick, G. Apai, and T. N. Rhodin, Phys. Rev. B **44**, 1880 (1991).
[40]A. Kuznetsova, I. Popova, V. Zhukov, J. T. Yates, Jr., G. Zhou, J. C. Yang, and X. Chen, J. Vac. Sci. Technol. A **19**, 1971 (2001).
[41]L. P. H. Jeurgens, W. G. Sloof, F. D. Tichelaar, and E. J. Mittemeijer, J. Appl. Phys. **92**, 1649 (2002).
[42]M. Cai, L. E. Levine, S. C. Langford, and J. T. Dickinson, Mater. Sci. Eng., A **400–401**, 476 (2005).
[43]D. Kuhlmann-Wilsdorf and H. Wilsdorf, Acta Metall. **1**, 394 (1953).
[44]H. Wilsdorf and D. Kuhlmann-Wilsdorf, Z. Angew. Phys. **4**, 418 (1952).
[45]V. V. Levitin, S. V. Loskutov, M. I. Pravda, and B. A. Serpetzky, Solid State Commun. **92**, 973 (1994).
[46]S. J. Basinski and Z. S. Basinski, *Dislocations in Solids* (North-Holland, New York, 1979), Vol. 4.
[47]L. P. H. Jeurgens, W. G. Sloof, F. D. Tichelaar, and E. J. Mittemeijer, Phys. Rev. B **62**, 4707 (2000).
[48]L. P. H. Jeurgens, W. G. Sloof, F. D. Tichelaar, and E. J. Mittemeijer, Thin Solid Films **418**, 89 (2002).